Review of Scientific Instruments

Back-focal-plane interferometric detection of nanoparticles in spatially confined microfluidic channels

Cite as: Rev. Sci. Instrum. **90**, 023107 (2019); https://doi.org/10.1063/1.5074194
Submitted: 22 October 2018 . Accepted: 01 February 2019 . Published Online: 20 February 2019

Abhay Kotnala, Yi Zheng, Jianping Fu, and Wei Cheng

AIP Publishing

Review of Scientific Instruments ARTICLE scitation.org/journal/rsi

Back-focal-plane interferometric detection of nanoparticles in spatially confined microfluidic channels

Cite as: Rev. Sci. Instrum. 90, 023107 (2019); doi: 10.1063/1.5074194
Submitted: 22 October 2018 • Accepted: 1 February 2019 •
Published Online: 20 February 2019

Abhay Kotnala,[1] Yi Zheng,[2] Jianping Fu,[2,3,4] and Wei Cheng[1,5,6]

AFFILIATIONS

[1]Department of Pharmaceutical Sciences, University of Michigan, 428 Church Street, Ann Arbor, Michigan 48109, USA
[2]Department of Mechanical Engineering, University of Michigan, 2350 Hayward Street, Ann Arbor, Michigan 48109, USA
[3]Department of Biomedical Engineering, University of Michigan, Ann Arbor, Michigan 48109, USA
[4]Department of Cell and Developmental Biology, University of Michigan Medical School, Ann Arbor, Michigan 48109, USA
[5]Department of Biological Chemistry, University of Michigan Medical School, Ann Arbor, Michigan 48109, USA
[6]Department of Biophysics, University of Michigan, Ann Arbor, Michigan 48109, USA

ABSTRACT

Nanoparticles are important in several areas of modern biomedical research. However, detection and characterization of nanoparticles is challenging due to their small size. Back-focal-plane interferometry (BFPI) is a highly sensitive technique that has been used in laser tweezers for quantitative measurement of force and displacement. The utility of BFPI for detection and characterization of nanoparticles, however, has not yet been achieved. Here we show that BFPI can be used for rapid probing of a suspension of nanoparticles in a spatially confined microfluidic channel. We show that the Gaussian Root-mean-squared noise of the BFPI signal is highly sensitive to the nanoparticle size and can be used as a parameter for rapid detection of nanoparticles at a single-particle level and characterization of particle heterogeneities in a suspension. By precisely aligning the optical trap relative to the channel boundaries, individual polystyrene particles with a diameter as small as 63 nm can be detected using BFPI with a high signal-to-noise ratio.

I. INTRODUCTION

Back-focal-plane interferometry (BFPI) is a highly sensitive technique that can measure laser deflection in a microfluidic chamber. Since its first quantitative description by Gittes and Schmidt,[1] BFPI has been used in conjunction with laser tweezers for a wide range of biophysical applications.[2–9] BFPI has high sensitivity, which was illustrated by its capacity to measure the angstrom level displacement of an optically trapped particle in ultrahigh-resolution optical tweezers' instruments.[10–12] In particular, methods based on BFPI have been developed to allow the routine calibration of optical tweezers' instruments.[13,14] However, very limited literature exists that explores BFPI for the detection and characterization of nanoparticles. Biological nanoparticles such as viruses or extracellular vesicles mediate many important processes in the development of diseases.[15,16] Similar to the cells where these particles are derived from, individual particles are likely to be highly heterogeneous in their compositions.[17] For example, differences just by a few molecules of envelope glycoproteins on the viral surface have a quantifiable effect on their biological infectivities.[18] To understand disease transmission by these particles,[19] it is essential to reveal this inter-particle heterogeneity. A technique that can measure these particles individually for their sizes and meanwhile, have the sensitivity to detect the inter-particle difference down to a single molecule, could be revolutionary.

We have recently extended the application of optical tweezers and BFPI for effective sizing and molecular characterization of biological nanoparticles such as viruses.[18,20,21] The encouraging data from these applications suggest that

BFPI may also be well suited for the detection and characterization of nanoparticles on a single-particle basis with high sensitivity, which is an area that has not been fully explored previously. We have recently developed a spatially confined microfluidic channel (MC) that can increase trapping frequency of nanoparticles by more than tenfold.[22] However the question that left unanswered remains the resolution of BFPI in resolving nanoparticles of varied size. The primary goal of the current study is to explore the use of the raw BFPI signal directly for rapid detection and characterization of nanoparticles of varied sizes. As we show, the time-domain BFPI can directly detect particle size heterogeneity with sufficient sensitivity and much reduced data acquisition time, in contrast to the frequency-domain analysis of BFPI data, which desires longer sampling time as we did in the past.[22] Thus, BFPI has the potential for ultrasensitive detection of nanoparticles and characterization of particle heterogeneity with high throughput.

II. EXPERIMENTAL SETUP

The current setup for BFPI was slightly modified from what we have reported previously.[23] The major modification is that a three-dimensional nanopositioning stage (NANO-3D200, Mad City Labs, Inc., WI) was installed on top of the existing micropositioning stage that was used to set up the microfluidic chamber. This modification allows us to steer the microfluidic chamber in three dimensions with nanometer precision and reproducibility. For a trapping laser, we use a tapered amplifier diode laser (SYS-420-830-1000, Sacher LaserTechnik LLC, Germany, λ = 830 nm in the air) focused by a 60× water-immersion objective (Nikon, N.A. = 1.2) for detection of nanoparticles, as schematically illustrated in Fig. 1(a), where the laser is indicated by a red shaded region inside a microfluidic channel (MC). Unscattered photons serve as an intrinsic reference field, which interferes with the photons scattered by the nanoparticle passing through the optical field. This label-free interference signal can be detected on a position-sensitive detector (PSD) (DL100-7PCBA3, Pacific Silicon Sensor, Inc., Westlake Village, CA) that is positioned at a plane conjugate to the back-focal-plane of the condenser. The PSD response is linear with respect to the centroid of the laser spot that impinges on the PSD. The trapping laser power at the focus was fixed at 130.8 mW and monitored using the PSD, which showed 1% variation throughout the experiments. The BFPI signal from a trapped particle was recorded at 62.5 kHz for 1 s. To enhance the nanoparticle trapping throughput, we use a microfluidic channel design to effectively direct nanoparticle flow paths through the laser focus region using a small cross-section channel, as shown in Fig. 1(b). The smallest section in this channel measures 10 × 10 × 50 μm^3 which can increase the trapping frequency by more than tenfold and thus allow for enhanced laser trapping efficiency and throughput.[22] We term this optical tweezers' system as an "active" trapping system since it uses an external influence of microfluidic flow together with narrow channel confinement to actively deliver target nanoparticles to the laser trap region, as compared to the "passive" trapping system where particles encounter the laser trap only through normal diffusion without external influences of flow, electric or magnetic field, etc.

In this "active" trapping system, two parameters are critical for the high-throughput of optical trapping: the nanoparticle flow velocity and the dimensions of the microfluidic channel cross section. Previously, we have demonstrated the need for an optimal nanoparticle flow velocity in this microfluidic channel.[22] Specifically, the nanoparticle flow rate needs to be high enough to help deliver particles to the trapping region and yet lower than the escape velocity of the particle to achieve the maximal trapping throughput. The small cross section of the microfluidic channel, on the other hand, helps focus nanoparticles to the laser trapping region and hence increase optical trapping throughput. To adjust the nanoparticle flow rate during the experiments, briefly, after injecting the nanoparticles in the microfluidic channel, a single nanoparticle was initially trapped in the microfluidic section containing the laser focus and then the flow rate was increased gradually by slowly increasing the applied pressure in the flow system. The flow rate was increased until the particle escaped the trap, which determined the cutoff pressure at which the flow rate equaled the escape velocity of the particle. Subsequent experiments were then performed slightly below this cutoff pressure to achieve the maximum throughput along with stable trapping of particles. The escape velocity for 403 nm and 184 nm polystyrene particles was 1820 ± 50 μm s^{-1} and 258 ± 10 μm s^{-1}, respectively, as we determined previously under identical laser trap settings.[22] Once a particle was trapped during our normal measurement routine, the BFPI signal was collected for 1 s and then the laser shutter was closed. This released the trapped particle instantly, which was flushed out due to the presence of the continuous flow in the microfluidic channel. Immediately after the release of the trapped particle, the laser trap was turned back on by opening the laser shutter to take the next measurement.

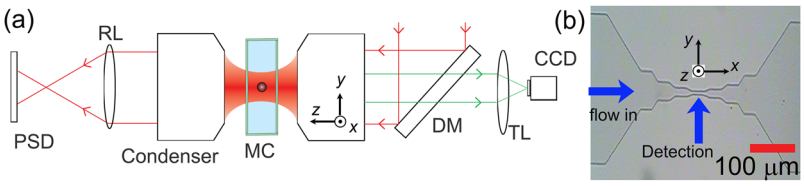

FIG. 1. Experimental setup. (a) Schematic optic layout for BFPI measurement. RL: relay lens; DM: dichroic mirror; TL: tube lens; and CCD: charge-coupled device. (b) Microscope image of the polydimethylsiloxane (PDMS) based microfluidic channel used for high-throughput trapping of nanoparticles. The xyz dimensions are shown, as indicated for each panel.

III. RESULTS AND DISCUSSION

A. Impact of laser focus positions on the BFPI signal in spatially confined microfluidic channels

In BFPI, unscattered photons serve as an intrinsic reference field, which interferes with the photons scattered by the trapped nanoparticles to yield a label-free signal that forms the basis of interference detection. Although the new microfluidic channel design [Fig. 1(b)] can trap particles at a throughput that is more than tenfold higher than that in a conventional microfluidic channel,[22] the sensitivity of BFPI in this channel has not been tested. Because the dimensions of this channel are much smaller than that of the conventional microfluidic channel used in laser tweezers,[24,25] one primary concern is the potential beam clipping by the confined channel dimension that may degrade the BFPI signal and thus its sensitivity. The potential beam clipping is illustrated in Fig. 2 in a cross-sectional view for both the conventional channel [Fig. 2(a)] and the confined microfluidic channel [Fig. 2(b)]. In a conventional channel, since the channel dimension is much larger than the dimension of the laser beam, the passage of the beam through the channel is unobstructed. By contrast, in the new microfluidic channel, the channel and the laser beam are comparable in their dimensions. Because the index of refraction of PDMS is different from that of glass, a slight translation of the beam focus along the channel depth will result in a beam clipping by the PDMS (for consistency, we will call z axis along the channel depth), and whether this has a measurable effect on BFPI is unknown. In fact, for a diffraction-limited Gaussian beam to be fully contained within a microfluidic channel, the following expression must be satisfied

$$w \geq h \tan\left(\sin^{-1}\frac{\mathrm{NA}}{n_m}\right), \tag{1}$$

where w is the microfluidic channel width, h is the channel depth, NA is the numerical aperture of the objective lens, and n_m is the refractive index of the medium (n_m = 1.33 for water-immersion objective lens). In other words, the minimal required width of the microfluidic channel w is a function of channel depth h. When the microfluidic channel becomes very thin ($h \leq 10\ \mu$m in our case), the channel section needs to have a minimal width to preserve the integrity of the laser beam passing through the channel.

To examine whether it is necessary to precisely align the laser beam relative to the channel boundaries in order to preserve the quality and sensitivity of BFPI, we have thus carried out systematic studies as presented below. The experiment is to trap a nanoparticle and then measure BFPI as a function of the beam position that is systematically varied along all three axes. To quantitatively assess any subtle changes in BFPI as a result of beam focus change, we compare three parameters of interest that are derived from BFPI, namely, the Gaussian root-mean-squared (RMS) noise calculated directly from the time-domain BFPI data over a duration of 1 s (i.e., one standard deviation of the raw data), the electronic diffusion coefficient (i.e., the translational diffusion coefficient measured from PSD recording in the unit of V^2/s), and the corner frequency extracted from the Lorentzian fit to the power spectrum of the BFPI signal, as we described previously.[21] To ensure the validity of experimental comparisons, experiments were performed swiftly in the following order: the experimentalist first traps a single polystyrene particle of 190-nm diameter and collects the BFPI data, and then steers a nanostage to change the laser beam focus inside the channel along a single axis. The BFPI data are then collected again from the same particle, until all locations have been measured using the same particle, which completes one set of the measurement. To examine the reproducibility of the above experimental design, the single particle was discarded after one experimental set and the above procedure was repeated two more times, each time using a new particle. The standard deviations were then calculated. Because the new microfluidic channel has sections of different widths [Fig. 1(b)], this study was performed for all the sections.

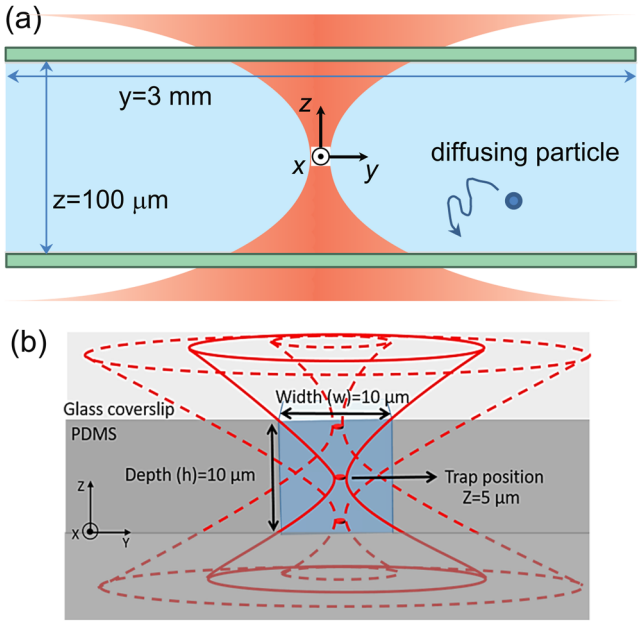

FIG. 2. Microfluidic channel designs used in current study. (a) The conventional channel design, in which the laser beam is depicted in red and (b) the new channel design, in which the laser beam is depicted in red, but hollow to indicate the impact of different positionings of the beam focus on the laser passage through the chamber. Both channels are shown in the same cross-sectional view, as indicated by the Cartesian axes. The dimensions of the channels are shown although not to the real scale.

1. Variation of the laser focus position along the Z axis, with fixed X and Y positions (condition 1)

For this condition, the laser focus position was systematically changed along the depth of the channel, i.e., along the Z direction, while the lateral position was fixed at the center along the length and width of each channel section in the X and Y directions, respectively. Once a single particle was trapped, the BFPI signal was recorded at a series of

Z locations by steering a nano-positioning stage. The channel boundaries along the Z direction, i.e., the water-PDMS (z = 0 μm) and glass-water (z ≈ 10 μm) interfaces, were predetermined by trapping a reference nanoparticle (190-nm) and slowly moving the stage along the Z direction, until the laser focus hits the channel boundary and the particle leaves the trap. Thus, accurate positions of the laser focus relative to the channel boundaries could be easily determined. Figure 3 shows the variation in the three parameters: Gaussian RMS noise, electronic diffusion coefficient, and corner frequency as a function of the Z-position inside the sections of different widths of the microfluidic channel. Because the same trapped particle was used to record the BFPI signal at different Z-positions for a given channel section, the variation in the three parameters should thus come from the change in laser focus position and not from the heterogeneity in the size of trapped particles. It is clear from the figure that all the three parameters start to deviate as the laser focus position is brought close to the channel boundaries along the Z axis. The deviation in the BFPI signal starts to appear at the laser focus position of approximately 3–4 μm away from the channel boundaries along Z and increases as it moves closer to the channel boundaries. Previously, Dufresne *et al.* have studied the Brownian dynamics of a microsphere between two parallel walls.[26] They found that both Faxén's law and a more general Stokeslet analysis could adequately describe the translational diffusion coefficient of the sphere. We also did the same analysis. We found that although both theories provided good description for the diffusion coefficient of the particle located in between 4 and 6 μm along the Z axis, they did not account for the data outside this middle zone. In conclusion, the change we observed in diffusion coefficients is not simply due to hydrodynamic interactions, but due to other issues such as beam clipping that we have suspected. Thus, based on this observation, it is necessary to precisely align the laser beam along the Z axis. A rule of thumb for reliable BFPI signal recording in the new microfluidic channel is to place the laser focus position more than 3–4 μm away from the channel boundaries in the Z direction. This minimizes the corruption of the BFPI signal from the laser-wall interactions and ensures faithful recording of interference data.

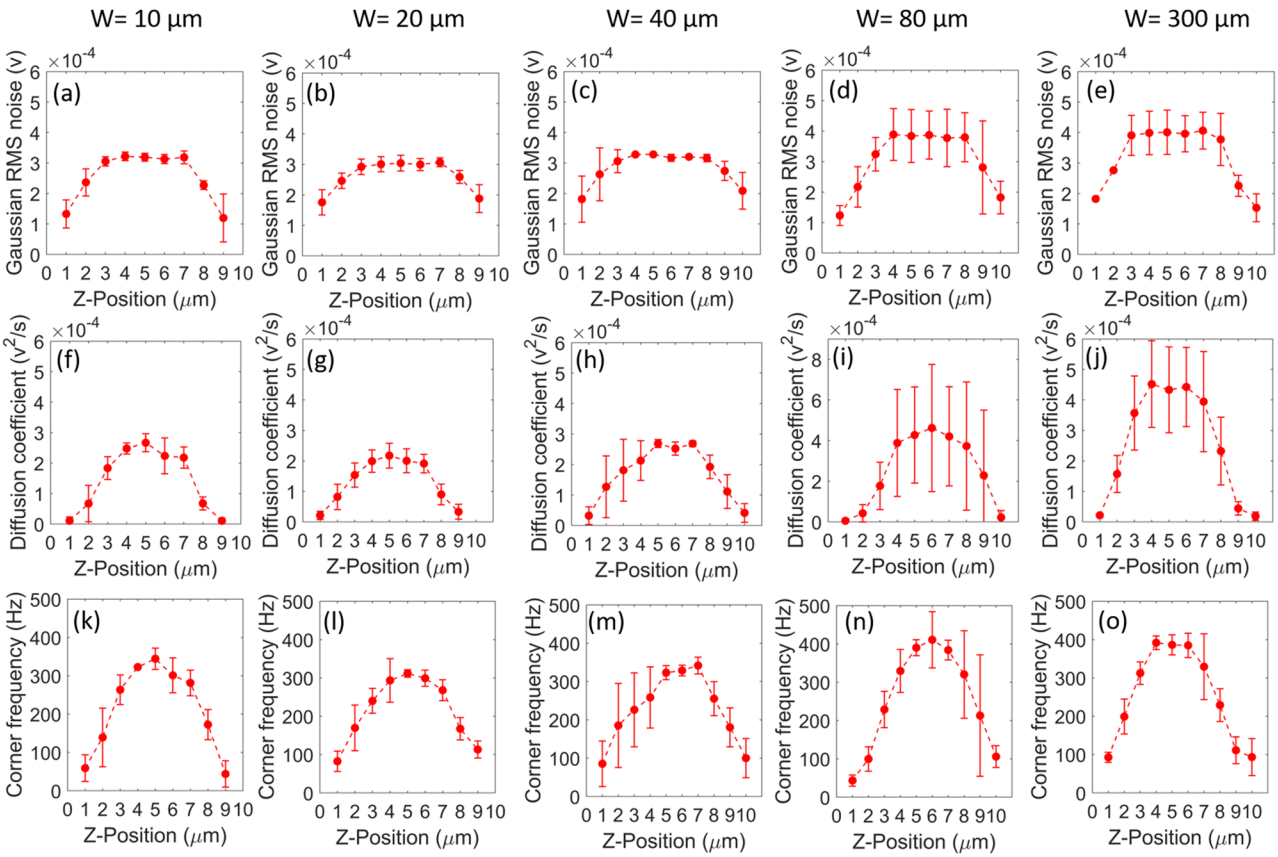

FIG. 3. [(a)–(e)] Gaussian RMS noise, [(f)–(j)] electronic diffusion coefficient, and [(k)–(o)] corner frequency at different Z-positions with 1 μm separation inside the channel for different channel sections of widths 10 μm, 20 μm, 40 μm, 80 μm, and 300 μm. The error bars represent the standard deviations from three independent repeats of the same measurement.

2. Variation of the laser focus position along the Y axis, with fixed X and Z positions (condition 2)

For this condition, the location of the laser focus was changed along the width of the channel in the Y direction, while its position along the X and Z directions was fixed at the center along the length and depth of the channel section, respectively. A 190-nm polystyrene particle was trapped and then moved to different Y locations using a nano-positioning stage, while the BFPI data were collected. The position of the channel boundaries along the Y-axis was determined directly from the bright field image of the microfluidic channel using a CCD camera, as shown in Fig. 1(b). Figure 4 shows the variation in the three parameters as a function of the Y-position of the laser focus inside the channel. Overall, less changes in these parameters were observed compared to condition 1 described above. However, they all showed deviations when the laser focus was positioned 3-4 μm away from the channel boundaries along the Y-axis, which was expected due to deflection of the laser beam by the channel boundary. Thus, it would be optimal to position the laser focus close to the center along the channel width, more than 3-4 μm away from the channel boundaries in the Y direction to prevent corruption of the BFPI signal arising from laser-wall interactions. This would result in faithful recordings of the interference data.

3. Variation of the laser focus position along the X axis, with fixed Y and Z positions (condition 3)

For comparison with the above two conditions (conditions 1 and 2), we also performed another set of measurements under condition 3. For this condition, the location of the laser focus was changed along the channel length in the X direction, while its position along the Y and Z directions was fixed at the center along the width and depth of each channel section, respectively. Based on our channel design as shown in Fig. 2(b), variation along the X-axis should not change the BFPI signal because no beam clipping can ever occur provided that the beam is focused at the center along both Y and Z axes. Thus, this measurement serves as an internal control for variations of BFPI signals that we have observed under the first two sets of conditions. To perform measurements under condition 3, the BFPI data from a trapped 190-nm polystyrene particle were recorded at different X-locations in each

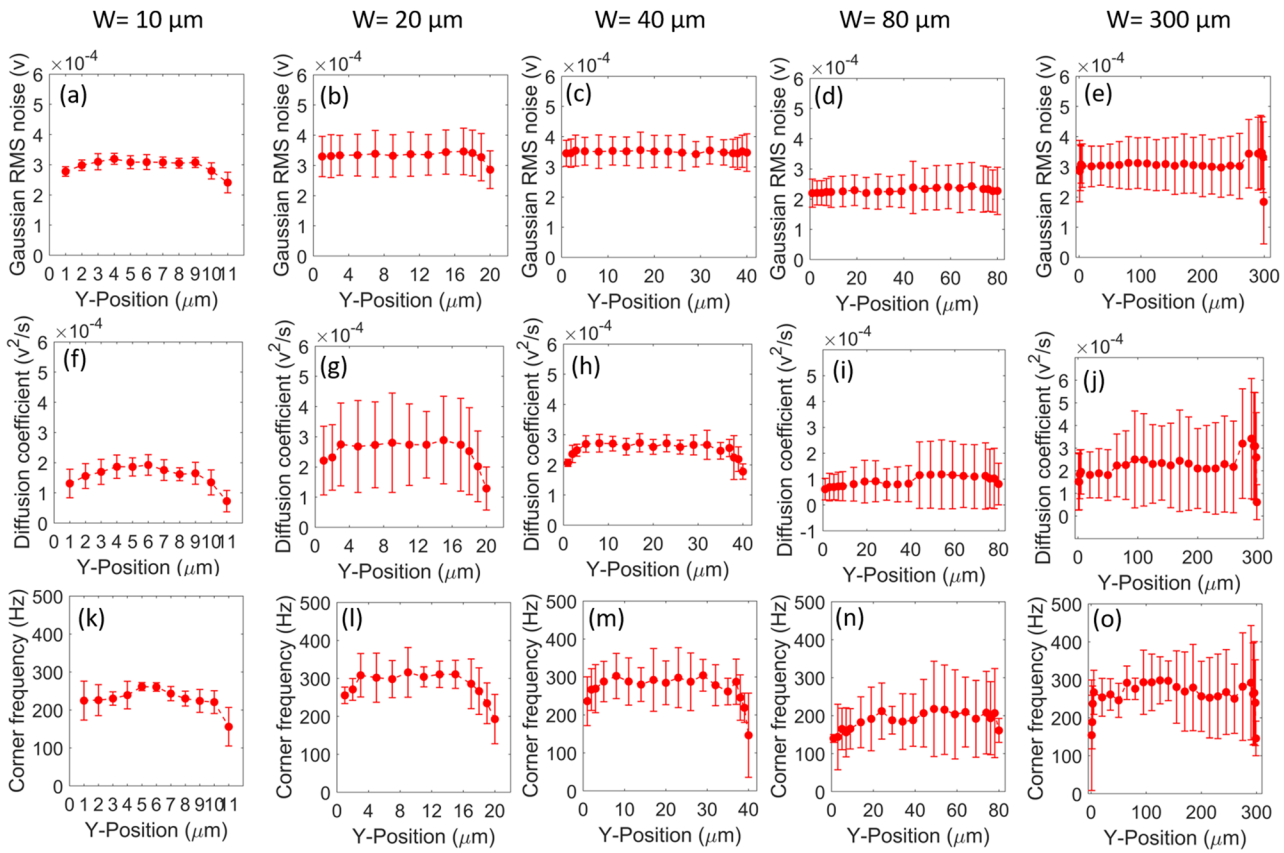

FIG. 4. [(a)–(e)] Gaussian RMS noise, [(f)–(j)] electronic diffusion coefficient, and [(k)–(o)] corner frequency at different Y- positions inside the channel for different channel sections of widths 10 μm, 20 μm, 40 μm, 80 μm, and 300 μm. The error bars represent the standard deviations from three independent repeats of the same measurement.

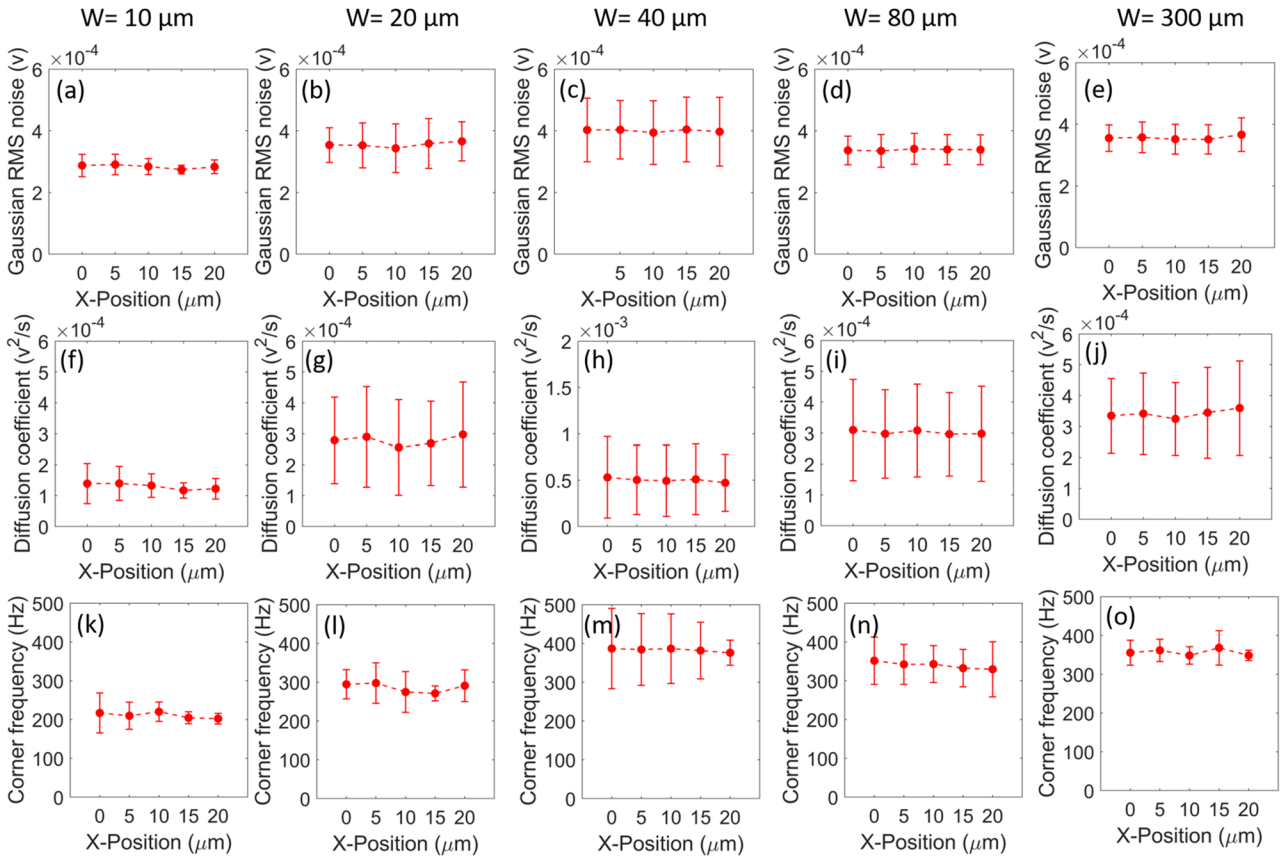

FIG. 5. [(a)–(e)] Gaussian RMS noise, [(f)–(j)] electronic diffusion coefficient, and [(k)–(o)] corner frequency at different X-positions with 5 μm separation inside the channel for different channel sections of widths 10 μm, 20 μm, 40 μm, 80 μm, and 300 μm. The error bars represent the standard deviations from three independent repeats of the same measurement.

section of the channel using a nano-positioning stage. Because each section has the same length of 20 μm, the laser focus was placed at five different locations with a spacing of 5 μm along the X axis. Figure 5 shows the variation in the three BFPI signal parameters as a function of the X-location inside the different microfluidic channel sections of varying width. It is clear from the figure that there is almost no change in the BFPI signal parameters as the laser focus position was changed along the length of the channel. This is also expected because based on Fig. 2(b), with Y and Z axes fixed constant, variation along the X axis should not result in any changes in beam interactions with channel walls. Thus, the variation along the X-position of the laser focus has no influence on the BFPI signal and therefore poses no restriction on positioning of the laser focus for faithful recording of the BFPI data. Finally, it is worth noting that the Gaussian RMS noise and diffusion coefficient that we report in Figs. 3–5 are both in voltage related units. In cases when these quantities in physical units are needed, i.e., m for the distance or m^2/s for the translational diffusion coefficient, a calibration routine should be carried out to determine the linear sensitivity of the detector as we have done in the past to convert volt to meter.[13,21] It is a procedure that is fully compatible with this newly designed microfluidic chamber as we showed recently.[22]

B. BFPI in high-throughput optical tweezers for rapid probing of size heterogeneity

Having systematically investigated the impact of beam locations relative to the channel boundaries on BFPI, we are set to determine the sensitivity of BFPI in detection of nanoparticles of varied sizes. To explore the precision and sensitivity of BFPI in nanoparticle detection, we conducted optical trapping experiments for a series of polystyrene particles of varied sizes. These reference particles (Spherotech, IL) have diameters ranging from 70 nm to 410 nm. To obtain an independent measurement for the size of these particles, we have also conducted transmission electron microscopy (TEM) studies on these particles, representative images of which are shown in Figs. 6(a)–6(d). To better simulate the real application of characterizing the size of unknown particles using BFPI, the size distribution for the 63 nm and 227 nm polystyrene particles was unknown during the experiments and was measured using TEM only after finishing the experiments. Through image analysis,[21] the mean diameter and standard deviation

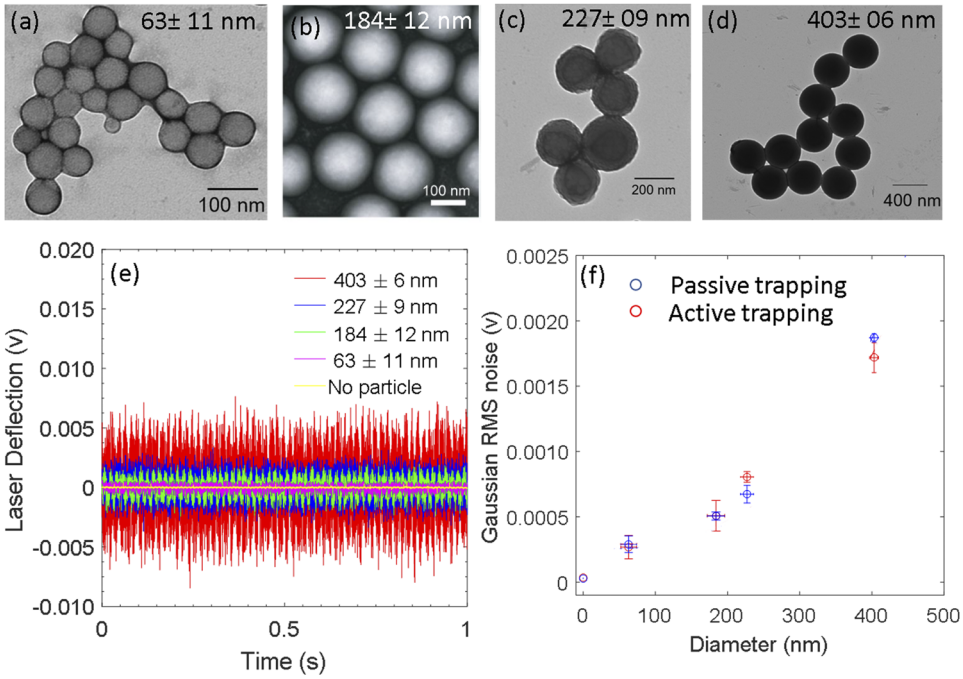

FIG. 6. [(a)–(d)] Representative TEM images of polystyrene particles used in this study. Scale bars are shown as indicated. (e) Representative BFPI signal from trapped polystyrene nanoparticles of mean sizes of 63 nm, 184 nm, 227 nm, and 403 nm. The yellow line represents the background BFPI signal with no particle in the trap. (f) Mean Gaussian RMS noise of the BFPI signal as a function of the mean diameter of polystyrene nanoparticles. Data collected from the high-throughput channel are shown in red circles, and data collected from the conventional channel are shown in blue circles. The error bars along the X-axis represent the standard deviations in the diameter of polystyrene particles from TEM measurements, with N = 100 for 63-nm particle, N = 72 for 184-nm particle, N = 100 for 227-nm particle, and N = 61 for 403-nm particle; the error bars along the Y-axis represent the standard deviation in the Gaussian RMS noise from BFPI measurements. The sample numbers for BFPI data collected in the high-throughput microfluidic channel are N = 97 for 63-nm particle, N = 95 for 184-nm particle, N = 108 for 227-nm particle, and N = 62 for 403-nm particle. The sample numbers for BFPI data collected in the conventional microfluidic channel are N = 65 for 63-nm particle, N = 93 for 184-nm particle, N = 110 for 227-nm particle, and N = 108 for 403-nm particle.

for each kind of polystyrene particle were 63 ± 11 nm (N = 100), 184 ± 12 nm (N = 72), 227 ± 9 nm (N = 100), and 403 ± 6 nm (N = 61). For optical trapping experiments, the individual bead stock was diluted with distilled and deionized water, sonicated for 1 min in a Cup Horn sonicator and then delivered into the microfluidic channel [Fig. 2(b)] for trapping. For optical trapping with high throughput, we used the channel section of 10 μm width to trap all the nanoparticles. To record unperturbed BFPI signals, the laser focus was carefully aligned and positioned at the center of channel in all three dimensions, as described below. First, the centroid of the focused laser spot was identified and marked on the image screen of an electron-multiplying charge-coupled device (EMCCD) camera. Then, the laser focus was positioned at the center of the channel in X and Y by aligning the center of the microfluidic channel image as shown in Fig. 1(b) with the centroid of the trapping laser beam. To position the laser focus at the center of the channel along the Z direction, we first located the left and right inner surfaces of the microfluidic channel [Fig. 1(a)] as followed. We trapped a reference particle at the laser focus in the microfluidic channel and slowly moved the microfluidic chamber along the Z-axis using a nanopositioning stage. The particle was bumped out of the trap as the laser focus touched either the left or the right inner surface of the microfluidic channel. The locations of both inner surfaces were noted and subsequently used as references to determine the center of the microfluidic channel along the Z-axis where the focus of the laser beam was positioned. When there were no particles in the optical trap, the BFPI signal was very "quiet" and stable, as shown by the thin yellow line in Fig. 6(e). By contrast, when a polystyrene particle of 63 nm mean diameter was trapped at the laser focus, the BFPI signal immediately became very noisy [the purple line in Fig. 6(e)], which could be clearly distinguished from the particle-free signal just by eye.

The origin of this noisy signal came from the interference between scattered and unscattered photons, which is a label-free signal. The repeated measurement for the same trapped single particle yielded BFPI data that were highly reproducible in amplitudes, with less than 1% coefficient of variance in the standard deviation of the data (data not shown), suggesting that under stable trapping conditions, BFPI has very high precision, consistent with our past experience on high-resolution optical trapping.[12,23] Time trajectories of 1 s duration from individual particles of other sizes are overlaid in Fig. 6(e), as indicated in the legend for particles of different sizes. It is clear that the amplitude of the BFPI signal is sensitive to the particle

diameter. Figure 6(f) plots the average Gaussian RMS noise calculated from 1-s data measured in confined microfluidic channels as a function of the mean particle diameter measured by TEM (red circles), which displays a monotonic increase of the Gaussian RMS noise with increasing particle size for this range of particles that we have investigated. The BFPI signal sensitivity was estimated to be 1.85×10^{-5} V/sqrt(Hz). This quantitative dependence suggests that BFPI has sufficient sensitivity to detect particles that are sub-100 nm in diameters. At a fixed power of 130.8 mW at the laser focus, we have not tried to trap particles smaller than 63 nm in diameter. However, it is conceivable that particles smaller than 63 nm diameter can be stably trapped by further increasing laser power at the focus. During BFPI measurements, we also observed some rare events ($N < 5$) with Gaussian RMS noise much larger than the majority of the events. For example, while conducting experiments with 184 nm polystyrene particles, we obtained some rare events with Gaussian RMS noise almost close to that of a single 403 nm polystyrene nanoparticle. We excluded such rare events in our mean RMS noise calculations because their RMS noise values were already above twofold of the expected RMS for a single particle. However, this observation suggest that the Gaussian RMS noise from a particle aggregate is likely indistinguishable from that of a single particle of larger size. Thus, additional parameters are necessary to distinguish a particle aggregate from a single particle of larger size.

The data shown in Figs. 6(e) and 6(f) were collected from the confined microfluidic channels. To confirm this quantitative dependence, we also conducted the same set of experiments in the conventional microfluidic channels [Fig. 2(a)] in which laser beam clipping was never an issue. These data are shown in blue circles in Fig. 6(f). Within error, these data are statistically indistinguishable from the data collected using the confined microfluidic channels and therefore confirm the quantitative dependence we have observed in the confined channels. The importance of the above data is twofold; first, it shows that the RMS noise that one can extract directly from the BFPI data can be used as a parameter to indicate nanoparticles of different sizes, provided that the index of refraction of these particles is the same; notably, optical trapping based BFPI has sufficient sensitivity to detect polystyrene particles smaller than 100 nm in diameter; second, the sensitive detection of nanoparticles can be carried out in the confined microfluidic channels to increase measurement throughput. To the best of our knowledge, this is the first work that has successfully utilized BFPI for discerning nanoparticles of different sizes. While other interferometry-based techniques have been reported in the literature for detection of nanoparticles either on a flat surface[27,28] or in a flow chamber,[29] BFPI has the unique potential for combination with highly sensitive single-molecule fluorescence for nanoparticle characterization.[21,30,31]

IV. CONCLUSION

BFPI has been frequently used in laser tweezers for calibration of photonic forces, although its sensitivity towards nanoparticles of different sizes has not been explored. In this work, we show that it is feasible to conduct BFPI measurement in narrowly confined microfluidic channels with high precision. The narrow channel dimension requires precise alignment of the laser relative to the channel sidewalls to avoid clipping of the laser beam. A systematic study was presented to investigate the impact of the confined channel on the BFPI signal, at different laser focus positions along all three dimensions inside the channel. Based on the study, we found that the laser focus position must be positioned approximately 3-4 μm away from the channel boundaries in both the Y and Z directions, for faithful recording of BFPI signals. The laser focus position along the X axis, i.e., along the channel flow direction had no impact on the BFPI signal. Once the laser focus position is properly aligned, the RMS noise of the BFPI signal has a quantitative dependence on particle size, thus providing a sensitive signal for detection of nanoparticles in suspension with high sensitivity.

ACKNOWLEDGMENTS

This work was supported by the National Institutes of Health (Grant No. 1R21AI135559-01A1 to W.C.), the Upjohn Research Award to W.C., and the National Science Foundation (CAREER Award Nos. CHE 1149670 to W.C. and CMMI 1536087 to J.F.).

REFERENCES

[1] F. Gittes and C. F. Schmidt, Opt. Lett. **23**, 7 (1998).
[2] L. Nugent-Glandorf and T. T. Perkins, Opt. Lett. **29**, 2611 (2004).
[3] F. Marsa, A. Farre, E. Martin-Badosa, and M. Montes-Usategui, Opt. Express **21**, 30282 (2013).
[4] M. Speidel, L. Friedrich, and A. Rohrbach, Opt. Express **17**, 1003 (2009).
[5] U. Bockelmann, P. Thomen, B. Essevaz-Roulet, V. Viasnoff, and F. Heslot, Biophys. J. **82**, 1537 (2002).
[6] C. Bustamante, W. Cheng, and Y. X. Mejia, Cell **144**, 480 (2011).
[7] I. Heller, G. Sitters, O. D. Broekmans, G. Farge, C. Menges, W. Wende, S. W. Hell, E. J. Peterman, and G. J. Wuite, Nat. Methods **10**, 910 (2013).
[8] M. W. Allersma, F. Gittes, M. J. deCastro, R. J. Stewart, and C. F. Schmidt, Biophys. J. **74**, 1074 (1998).
[9] Y. Gao, S. Zorman, G. Gundersen, Z. Xi, L. Ma, G. Sirinakis, J. E. Rothman, and Y. Zhang, Science **337**, 1340 (2012).
[10] E. A. Abbondanzieri, W. J. Greenleaf, J. W. Shaevitz, R. Landick, and S. M. Block, Nature **438**, 460 (2005).
[11] J. R. Moffitt, Y. R. Chemla, D. Izhaky, and C. Bustamante, Proc. Natl. Acad. Sci. U. S. A. **103**, 9006 (2006).
[12] W. Cheng, S. G. Arunajadai, J. R. Moffitt, I. Tinoco, Jr., and C. Bustamante, Science **333**, 1746 (2011).
[13] S. F. Tolic-Norrelykke, E. Schaffer, J. Howard, F. S. Pavone, F. Julicher, and H. Flyvbjerg, Rev. Sci. Instrum. **77**, 103101 (2006).
[14] K. Berg-Sorensen and H. Flyvbjerg, Rev. Sci. Instrum. **75**, 594 (2004).
[15] B. N. Fields, D. M. Knipe, and P. M. Howley, *Fields Virology* (Wolters Kluwer Health/Lippincott Williams & Wilkins, Philadelphia, 2007).
[16] S. E. Andaloussi, I. Mager, X. O. Breakefield, and M. J. Wood, Nat. Rev. Drug Discovery **12**, 347 (2013).
[17] P. G. Schiro, J. C. Gadd, G. S. Yen, and D. T. Chiu, J. Phys. Chem. B **116**, 10490 (2012).
[18] M. C. DeSantis, J. H. Kim, H. Song, P. J. Klasse, and W. Cheng, J. Biol. Chem. **291**, 13088 (2016).
[19] N. F. Parrish, F. Gao, H. Li, E. E. Giorgi, H. J. Barbian, E. H. Parrish, L. Zajic, S. S. Iyer, J. M. Decker, A. Kumar, B. Hora, A. Berg, F. Cai, J. Hopper,

T. N. Denny, H. Ding, C. Ochsenbauer, J. C. Kappes, R. P. Galimidi, A. P. West, Jr., P. J. Bjorkman, C. B. Wilen, R. W. Doms, M. O'Brien, N. Bhardwaj, P. Borrow, B. F. Haynes, M. Muldoon, J. P. Theiler, B. Korber, G. M. Shaw, and B. H. Hahn, Proc. Natl. Acad. Sci. U. S. A. **110**, 6626 (2013).
[20]Y. Pang, H. Song, and W. Cheng, Biomed. Opt. Express **7**, 1672 (2016).
[21]Y. Pang, H. Song, J. H. Kim, X. Hou, and W. Cheng, Nat. Nanotechnol. **9**, 624 (2014).
[22]A. Kotnala, Y. Zheng, J. Fu, and W. Cheng, Lab Chip **17**, 2125 (2017).
[23]W. Cheng, X. Hou, and F. Ye, Opt. Lett. **35**, 2988 (2010).
[24]S. B. Smith, Y. Cui, and C. Bustamante, Methods Enzymol. **361**, 134 (2003).
[25]S. B. Smith, Y. Cui, and C. Bustamante, Science **271**, 5250 (1996).
[26]E. R. Dufresne, D. Altman, and D. G. Grier, Europhys. Lett. **53**, 264 (2001).
[27]K. Lindfors, T. Kalkbrenner, P. Stoller, and V. Sandoghdar, Phys. Rev. Lett. **93**, 037401 (2004).
[28]G. G. Daaboul, A. Yurt, X. Zhang, G. M. Hwang, B. B. Goldberg, and M. S. Unlu, Nano Lett. **10**, 4727 (2010).
[29]F. V. Ignatovich and L. Novotny, Phys. Rev. Lett. **96**, 013901 (2006).
[30]X. Hou and W. Cheng, Opt. Lett. **36**, 3185 (2011).
[31]X. Hou and W. Cheng, Biomed. Opt. Express **3**, 340 (2012).